# A Planar Milli-Robot System on an Air Bearing *

Ronald S. Fearing
Department of EE&CS
University of California
Berkeley, CA 94720
email: ronf@eecs.berkeley.edu

## 1 Introduction

For assembly and testing purposes, for example, assembly or testing of hybrid circuit modules, millimeter and smaller size objects need to be transported over distances on the order of several object diameters. In order to handle these submillimeter size mechanical or electronic components, a miniature manipulator system has been developed. There are many advantages to shrinking robots and mechanical actuators to the same size as the parts to be manipulated. Extremely delicate forces can be applied, robots can be readily parallelizable, and the relative accuracy required can be markedly reduced. One of the major difficulties in building millimeter scale microrobots is overcoming forces due to friction and wiring. Friction forces can be reduced by using levitation or using fluid lubrication, such as an air-bearing. This paper considers some initial steps towards implementing a miniature robotic system using magnetically driven platforms about 7 mm square on a 35 mm square workspace. The position of the platform is sensed using an array-type capacitive proximity sensor. The system should be scalable to one tenth the present size. The mobile platforms can be used in cooperation to grab and position small objects.

When parts to be handled are less than one millimeter in size, adhesive forces between gripper and object can be significant compared to gravitational or inertial forces. These adhesive forces arise primarily from surface tension, Van der Waals, and electrostatic attractions and can be a fundamental limitation to part handling in a gas environment. While it is possible to fabricate miniature versions of conventional robot grippers, for example from polysilicon, it appears that it will be difficult to overcome adhesion effects for the smallest parts. Thus, manipulation of parts on the order of 10 micron or smaller may best be done in a fluid medium. Figure 1 shows a typical concept for a planar milli-manipulator system. It can be thought of as a miniature version of the RobotWorld system (see for example [Ish-Shalom, 1994] for a description of some current RobotWorld research). I believe Prof. H. Fujita is one of the main originators of the minia-

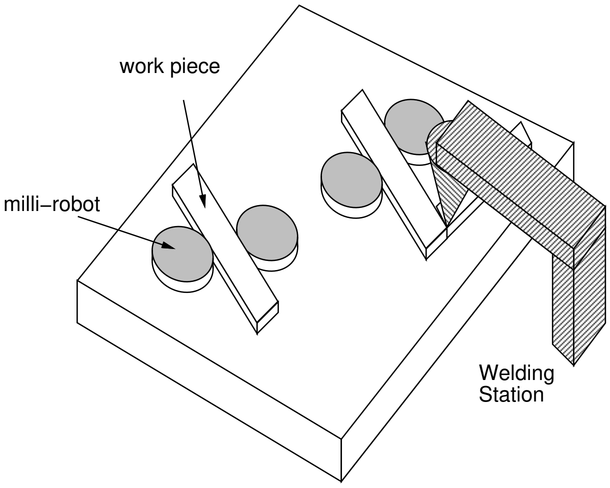


Figure 1: Generic model of miniature planar robotic workcell. The goal is to build a system on which miniature parts can be transported, tested, and assembled.

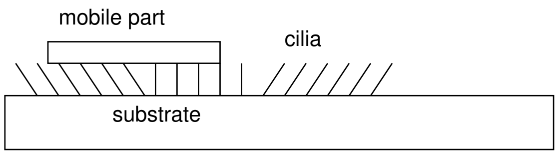


Figure 2: Part transport by cilia on active surface. Exact motion depends on model of friction properties.

*This work was funded in part by: NSF-PYI grant IRI-9157051.

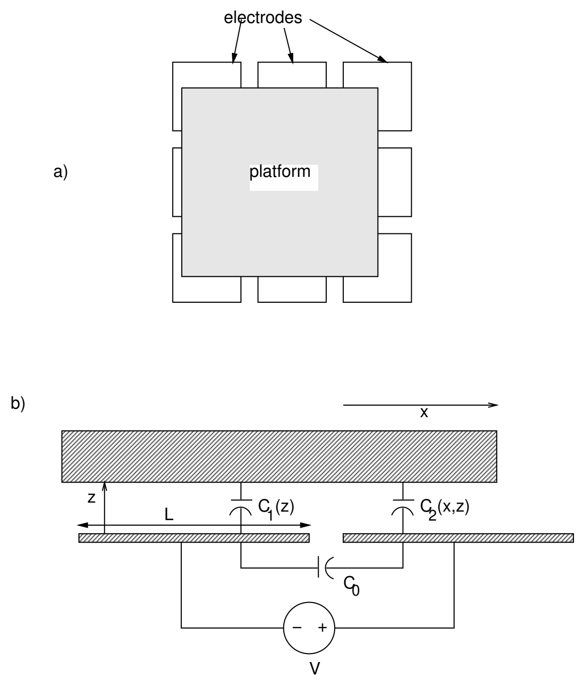


Figure 3: Planar electrostatic drive with levitated platform. a) Electrode configuration. b) Equivalent circuit.

ture planar manipulator system concept [Fujita and Omodaka, 1987; Fujita 1989]. There are two basic types of systems-the active surface where motion of the surface applies mechanical forces to any objects on the surface, and the electromagnetic type where parts and pushing elements can be driven by magnetic or electrostatic forces.

A typical example of an active surface is the "cilia" type drive of Figure 2. By coordinated wave gaits of cilia, parts can be transported in any direction on the surface [Fujita and Gabriel, 1991]. It is possible that sticking effects between cilia and parts in a non-liquid environment could cause indeterminate behavior [3, 2, 19, 20]. There have been a wide variety of actuation schemes for cilia, including thermal [Ataka et al 1993], ultrasonic [Furuhata Hirano Fujita 1991], electrostatic [Boehringer et al 1994], and magnetic [Liu and Will, 1995] using magnetic flap actuators developed by [Liu, Tsao and Tai, 1995].

Due to large friction forces on small dry parts, a fluid medium and lubrication (either gas or liquid) is commonly used. For example, whole silicon wafers on a gas bearing can be driven electrostatically [Tokisue et al 1991]. Another type of active surface uses controlled jets of air to push parts around. This method is used in semiconductor wafer transport and has been prototyped at the micro scale [Konishi and Fujita 1993]. Alternative methods to avoid problems with friction include levitation due to the Meissner effect [Fujita, 1989], [Kim, Katsurai, Fujita 1990] [Maeda, Aihara, Fujita 1993] and a partially levitated motion phase for a miniature magnetic actuator [Busch-Vishniac et al 1990], [Wang et al, 1991]. Other possibilities are active magnetic levitation [Robichaux and Ahmed, 1992], or self-pressurized air bearings [Fearing, 1992]. With some magnetic actuators, the forces are strong enough to overcome friction, and lubrication is not essential [Wagner et al 1993], [Inoue et al 1995].

Biological cells in a liquid medium can be moved by electrostatic attraction. Integrated systems using arrays of electrodes to apply electrostatic fields have been used to transport and fuse cells [Fuhr, et al 1991; Sato et al, 1990; Washizu, 1990]. Sensing systems can also be integrated to determine cell position. Dry particles can also be moved by AC potentials [Moesner and Higuchi, 1995]. As some objects may be damaged by high electric fields, mechanically driven transport systems are also needed.

An integrated system for manipulating dry parts in the plane using multiple mobile manipulation units was proposed by Pister et al [1990]. This device consists of a 1 $cm^2$ substrate with an air bearing to support individual $1mm^2$ platforms. The individual platforms are driven in the plane by electrostatic forces (see Figure 3), and could carry grippers, probes for sensing, or tools for processing. (To be useful, silicon micro-robots will need tools to interact above the plane of the wafer, not just in it. One promising approach, called "silicon origami" [Suzuki et al, 1992] or micro-hinges [Pister, et al 1992] allows planar fabrication, followed by 3 dimensional assembly of structures.) By incorporating capacitive position sensing of the platforms, an integrated micro system for parts handling could be made on a single chip.

## 1.1 Actuation Methods

One scaling law that is helpful for micro-actuators is the increased break-down field strength of very small gaps due to the Paschen effect. Thus for small sizes, the obtainable electrostatic forces can be stronger than electromagnetic forces [Trimmer and Jebens, 1989], [Price et al, 1989].

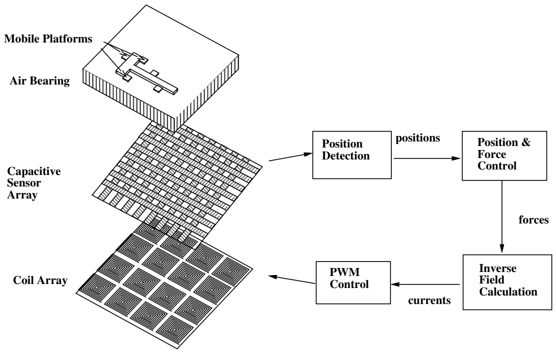


Figure 4: Planar milli-robot system block diagram. Positions of robots and parts are detected using capacitive sensing, and robots are driven magnetically. The servo rate is 120 Hz, limited by sensor electronics scan time. The sensor is an 8 by 8 array, and the electromagnets are a 6 by 6 array.

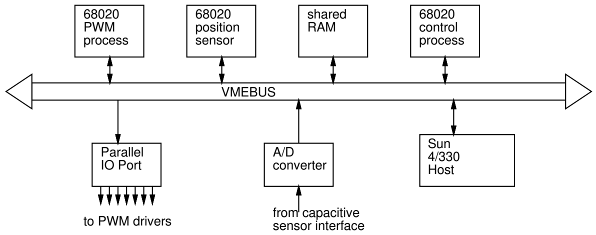


Figure 5: Multiprocessor system for milli-robot control. Two processors are dedicated solely for sensor and PWM processing, and a third processor implements the control algorithm.

Unfortunately, electrostatic actuation may have problems with charge accumulation in the dielectric, see for example [Anderson and Colgate, 1991]. Another problem is that an electrostatic drive won't work in a conductive fluid medium such as water. Magnetic actuation may thus be an attractive alternative, see for example [Busch-Vishniac, 1991]. Recently, magnetic actuators have been made at the micro-scale using extensions of micromachining techniques, see for example [Ahn et al 1993], [Guckel et al 1993] [Wagner and Benecke, 1991], [Wagner et al 1991]. Comprehensive surveys of available actuator technology and scaling effects have been published [Dario et al 1992], [Fujita and Gabriel, 1991], [Shimoyama, 1995], [Trimmer and Jebens, 1989].

## 2 System Description

As parts become small, the inertial forces become negligible while the friction forces and electrostatic forces can become very large. An air bearing works very well at the macro and micro scales to reduce friction. To avoid constructing a miniature air bearing with thousands of air holes, a self-pressurizing squeeze-film air bearing is used. Since the bearing gap is less than about $5\mu m$, surfaces must be very clean and very flat for the bearing to function properly.

The design considered in this paper uses a mobile platform made from high permeability or magnetic material, with embedded coils in a stator. The forces required for translation of the platform are very low, so even low strength magnetic fields may work well. Magnetics may also be attractive when using an internal high-current low-voltage source like a single cell battery, since the coil will usually be fairly low impedance.

It is useful to be able to sense the position of both driven platforms and passive parts floating on the air bearing. For example, magnetically driven platforms could be used to push and grasp passive pieces of silicon which are not controlled by the magnetic fields. Capacitive sensing is used to detect the presence and position of dielectrics and conductive materials. Of course a vision system could be used for platform position detection, [Inoue et al 1995] but the frame rate is typically fairly low at 60 Hz, and optics can limit the workspace for vertical assembly operations. Figure 4 shows the overall view of the milli-robot system, with the closed loop control system shown in Figure 5. Conventional printed circuit techniques, with a resolution of $75\mu m$ are used to fabricate the sensor and electromagnet arrays. The sensor and magnet layers are glued together, and a thin piece of cover glass is used for the bottom surface of the air bearing. The circuit board layers are then glued to a rigid backing plate and a piezoelectric driver to form the complete mechanical system (Figure 6). (The vertical axis in the figure is not to scale). It is interesting to note that there is no precision assembly required other than ensuring that the cover glass is flat to within $2\mu m$. The mobile platforms are simply square or round pieces of silicon or glass with a magnet glued on.

The 7.5 mm diameter platforms float on a self-pressurized air bearing created by the squeeze-film effect between the platform and glass covering the capacitive sensor array. The capacitive sensor array and magnetic coil array are fabricated on $250\mu m$ thick printed circuit board mate-

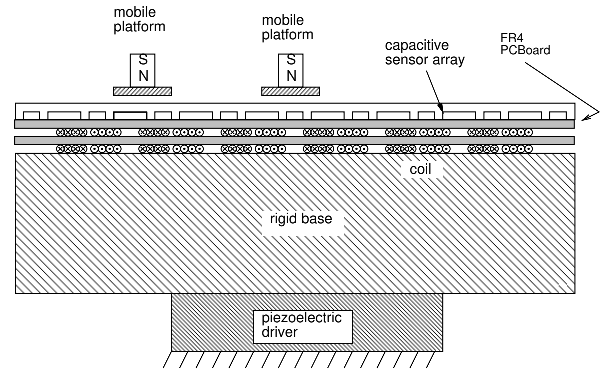


Figure 6: Overall construction of milli-robot system.

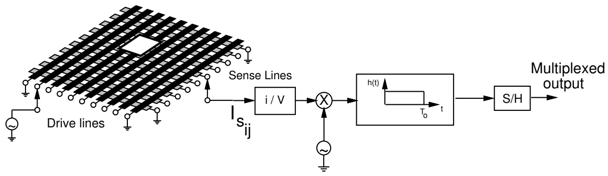


Figure 7: Position sensor array and interface electronics. Sensitivity of the electronics is about $5 \times 10^{-16} F$ at 120 Hz bandwidth.

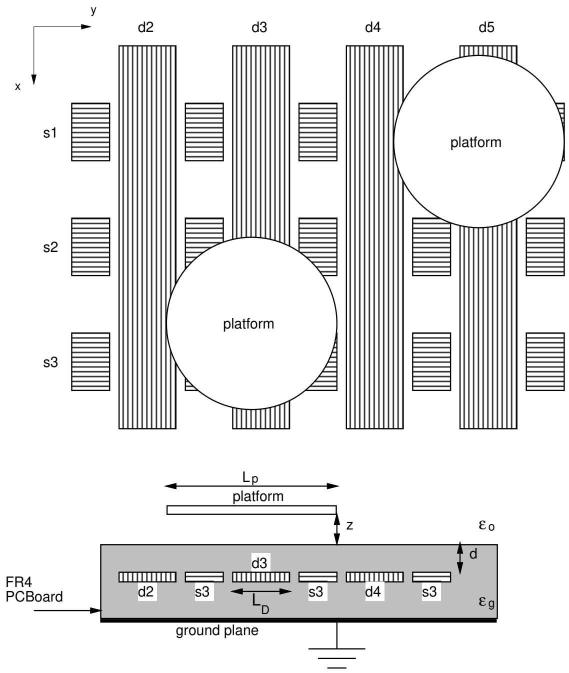


Figure 8: Geometry for calculating sensor capacitances. Platform is 7.5 mm wide, drive and sense line width is approximately 2.5 mm.

rial chosen to reduce the gap distance for the magnetic field. A rigid aluminum base, approximately 1 cm thick, is used to reduce flexible bending modes. A piezo-electric driver moves the whole assembly vertically at 20 KHz with an amplitude of approximately 10 nm, giving a calculated air bearing thickness of about $5 \mu m$.

# 3 Capacitive Position Sensing Array

The capacitive position sensor consists of an array formed by 8 driven electrodes running perpendicular over 8 sense electrodes, as depicted in Figure 7. The array is covered with approximately $1.5 \times 10^{-4} m$ of glass to give a smooth surface for the air bearing. A 250 KHz sine wave is injected into one of 8 drive lines, and the capacitive coupling current is measured on one of 8 sense lines. The array is scanned at a 120 Hz frame rate, with unaddressed rows and columns being grounded. Stray capacitance to ground on the sensor output, for example cable capacitance, is suppressed using a current-to-voltage converter. The current to voltage converter ideally has zero input impedance. A synchronous demodulator is used to measure the magnitude of the coupling current. The sensor easily measures a capacitance change of 1 part in 1000. The capacitive sensor has rows and columns spaced at $2.5 \times 10^{-3} m$ .

The coupling currents from the sensor will be a function of the conductive and dielectric properties and position of objects resting above the sensor surface. The sensing array can be used to detect the position of a platform as shown in Figure 8. The mobile platform consists of a 7.5 mm diameter conductive plate. (The coupling current is maximized by using a small conductive platform). The actual top layer circuit board used is shown in Figure 9. Other approaches to planar capacitive sensors can be found in [Bonse et al 1994] and [Miller, 1990].

## 3.1 Height Measurement

With the platform directly centered above one sense line and one drive line (that is, no overlap with other sense or drive lines), the float height can be found as a function of the measured currents. Let $I_o'$ be the sensed current when the platform is on the substrate, and let $I_f'$ be the current when the platform is floating, with air gap permittivity $\epsilon_o$, and the permittivity of the

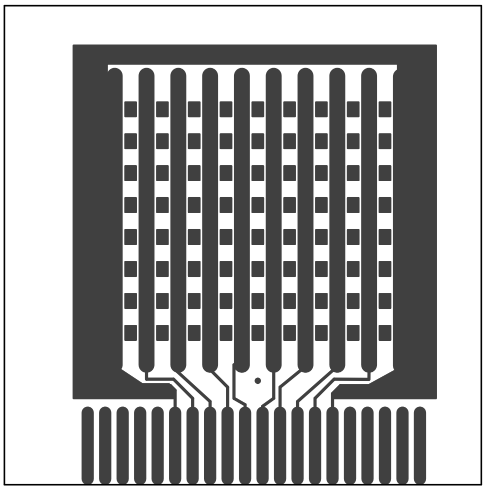

Figure 9: Circuit board layout for capacitive sensor array. Element spacing is 2.5 mm.

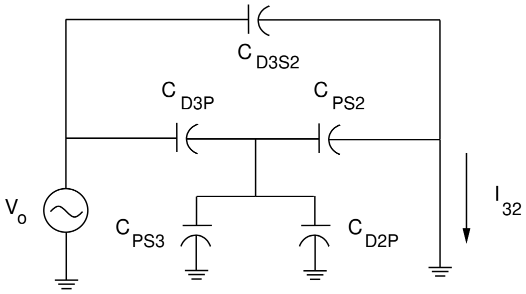


Figure 10: Equivalent circuit for capacitive sensor array. Fixed coupling capacitance $C_{D3S2}$ is subtracted as an offset. Capacitance is measured with a current amplifier at virtual ground, so shielding capacitance can be neglected.

covering layer of glass $\epsilon_g \approx 4.8\epsilon_o$ . The height of a square platform can be determined from

$$z = \frac{\epsilon_o}{\epsilon_g(2L_P - L_D)}\left(\frac{1}{I_f{}'} - \frac{1}{I_o{}'}\right), \qquad (1)$$

where $L_P$ and $L_D$ are the width of the platform and drive electrode respectively.

## 3.2 Position Measurement

With the platform as shown in the figure, the equivalent electrical circuit is shown in Figure 10 when column 3 ("D3") is driven, and row 2 ("S2") is sensed. Let $I_Sij$ be the sensed current when drive $i$ is driven, and sense $j$ is read. Note that for this configuration, the unused grounded lines D2 and S3 drain off coupling current from $I_{S32}$. Scanning all 4 combinations, the sensed currents are given by

$$I_{Sij} = \frac{C_{DiP}C_{PSj}}{C_\Sigma} j\omega V_o \qquad (2)$$

where $C_\Sigma = C_{Di} + C_{Di+1} + C_{Si} + C_{Si+1}$ plus any additional capacitance to the platform.

An earlier version of this paper [Fearing 1992] considered measuring the position of square platforms. However, the orientation of a platform is not directly controlled in this system, so a circular platform is preferred as there are only 2 degrees of freedom to sense. The capacitance between the platform and drive and sense lines can be approximated as a parallel plate capacitor. Thus the capacitance from the platform to drive strip 1 is given by

$$C_{D1P} = \frac{\epsilon_o\epsilon_g g(y)}{\epsilon_o d + \epsilon_g z}, \qquad (3)$$

where $g(y)$ is the area of intersection between the drive line and the circular platform for the platform at relative position $y$, and $d$ is the glass layer thickness, about $150\mu m$. Similarly, the capacitance from platform to drive strip 2 is

$$C_{D2P} = \frac{\epsilon_o\epsilon_g g(y - 2L_D)}{\epsilon_o d + \epsilon_g z}, \qquad (4)$$

where $L_D$ is the drive line width. After some algebra, it can be shown that the current ratio

$$\frac{I_{D1S1} + I_{D1S2}}{I_{D2S1} + I_{D2S2}} = \frac{g(y)}{g(y-2)}. \qquad (5)$$

This ratio is approximately a parabola, thus the relative position can be obtained through the square root of the current ratio.

Extracting the $x$ position is slightly more complicated, as there is coupled dependence on $x$ and $y$. The capacitance from platform to sense lines is proportional to the intersection of a circle with two squares:

$$C_{PS1} = \frac{\epsilon_o\epsilon_g h(x,y)}{\epsilon_o d + \epsilon_g z}, \qquad (6)$$

where $h(x,y)$ is the area of intersection of the sense line with the circular platform. Similarly for sense line 2,

$$C_{PS2} = \frac{\epsilon_o\epsilon_g h(x - 2L_D, y)}{\epsilon_o d + \epsilon_g z}. \qquad (7)$$

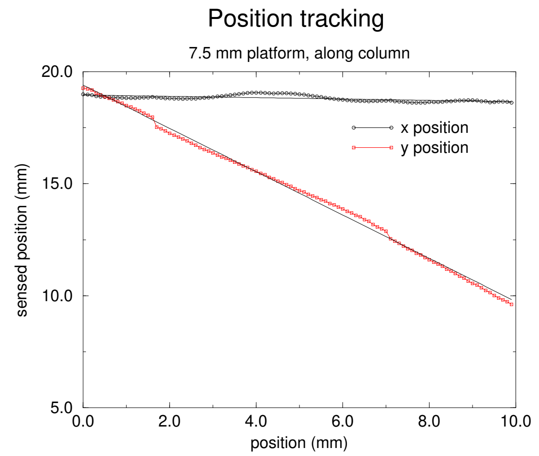


Figure 11: Position estimation for motion in y direction.

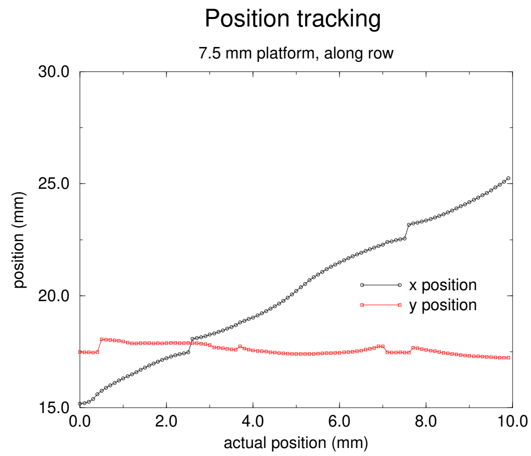


Figure 12: Position estimation for motion in x direction.

After some algegra, it can be shown that the current ratio

$$\frac{I_{D1S1}+I_{D2S1}}{I_{D1S2}+I_{D2S2}} \tag{8}$$

is equivalent to

$$\frac{h(x,y)[g(y)+g(y-2L_D)+h(x-2L_D,y)]}{h(x-2L_D,y)[g(y)+g(y-2L_D)+h(x,y)]}. \tag{9}$$

This current ratio can be approximated as a separable function of $x$ and $y$, and solved for $x$ given the $y$ position obtained above. This is the basic form of the equations for determining relative platform displacement. There are actually four different configurations of the platform, depending on how it is centered with respect to the array.

The current ratio is generally a well-behaved measure, which has the advantage of eliminating dependencies on dielectric constants and the float height. (Note that the float height is not constant, and is a function of the magnetic field strength). Before the current ratio method can be used, the offset current is subtracted from each sensed current. Preliminary experiments were performed to evaluate the position sensing algorithm. In the experiment, a micrometer stage with $10\mu m$ accuracy was moved in $100\mu m$ steps while a 7.5 mm diameter platform was levitated on the air bearing to remove friction effects, and maintain constant height. The platform was moved using a permanent magnet attached to the micrometer stage. Results are shown in Figure 11 and Figure 12. Several imperfections are apparent, particularly the discontinuities at 5.1 mm spacing which corresponds to the sensor element spacing. A detailed examination of the discontinuities has shown that they result from coupling of the fringing fields which have been ignored in the parallel plate model. A slightly larger platform could reduce this problem. The sensed $x$ position is more problematic; the separable approximation used for inverting equation 8 is a likely source of the problem. While the accuracy of the sensing algorithms needs improving, the resolution of the sensor is reasonable, with standard deviation better than $10\mu m$ with the coils off.

Further refinements, such as embedding a more complicated conductor pattern in the platform could be used to determine rotation angle as well. More general purpose capacitive imaging algorithms are also needed which can accurately determine the position and orientation of arbitrary polygons in the plane.

# 4 Fluid Bearings for Platform Levitation

A stable and relatively stiff fluid bearing is essential to ensure smooth operation of the mobile platform. If the rotational stiffness is too low, the platform could tilt and touch down, probably sticking to the surface. With some actuation methods, for example, a linear variable-capacitance motor, the normal force into the substrate may be 100 times greater than the tangential drive force. The more common approach to an air bearing uses an external air supply. However, for small dimensions and narrow air gaps, a form of self-pressurization can be obtained by us-

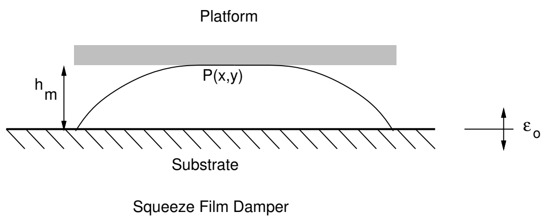


Figure 13: Squeeze film bearing. High frequency vibration of the substrate compresses air in the narrow gap between the platform and substrate.

ing a squeezed film of gas. This section examines the feasibility of using the squeeze film to support the platform.

## 4.1 Externally Pressurized Bearing

An air bearing can be constructed using surface micro-machining as described by [Pister et al, 1990]. That bearing had an array of 10 $\mu$m air nozzles spaced at 100 $\mu$m intervals. Each nozzle was made by a plasma etch through a 1 $\mu$m membrane, and ran with a supply pressure of approximately 500 pascals. Several platforms up to 750 $\mu$m thick were supported on this bearing, with float heights of about 20 $\mu$m. The low nozzle resistance and low supply pressure tend to encourage this high float height. For electrostatic drive, the equilibrium height should ideally be less than 10$\mu$m to increase the drive force on the platform.

## 4.2 Squeeze Film Bearing

A squeeze film bearing action is defined by [Pan and Broussard, 1967]:

- *In a squeeze film bearing, high frequency transverse oscillations of one of the bearing surfaces provides a pumping action. The oscillatory squeeze motion results in a time-averaged pressurization effect primarily due to the compressibility of the gas film, and the degree of this pressurization increases monotonically with the amplitude of the oscillation relative to the average gap.*

The intuition behind a squeeze film bearing can be improved by the following example. Consider two square flat plates with a very thin layer of air in between them. If these two plates are brought together slowly, the air between them will escape out the sides of the plates, and the two plates will touch. If the two plates are brought rapidly together, the gas will not all have time to escape, and will be compressed in the central region, increasing the fluid pressure there. Now consider a floating platform at average height $h_m$ above a rapidly vibrating substrate as shown in Figure 13, driven by $z(t) = e_o cos\omega t$. The acceleration of the substrate is thus $-e_o\omega^2 cos\omega t$. Suppose the pressure under the platform is slightly less than the normal load on the platform, then the platform will start to decrease in height. However, when the substrate moves up on the next cycle, the fluid will be more compressed since the gap is now smaller, increasing the pressure under the platform, and forcing it back up to its equilibrium height.

Assuming constant fluid density, Reynold's equation for compressible gas film lubrication is [Sherman, 1990]:

$$\vec{\nabla}\cdot[(\frac{h^3}{\mu})\vec{\nabla}p] \;=\; 12\frac{\partial(h)}{\partial t} \;+\; 6\vec{\nabla}\cdot(hU) \qquad (10)$$

where $h$ is the height, $p$ is pressure, and $U$ is velocity. If the variations in pressure $\delta p$ are small compared to $P_a$, the ambient pressure, then in linearized form [Blech, 1983]:

$$\frac{h_m^2 P_a}{12\mu}\nabla^2\frac{\delta p}{P_a} \;-\; \frac{\partial}{\partial t}\frac{\delta p}{P_a} \;=\; \frac{\partial}{\partial t}\frac{e_o\cos\omega t}{h_m}. \qquad (11)$$

This linearized version can be solved for sinusoidal excitation in the steady state using a series solution. The first term of the series solution gives the fundamental mode response. The in-phase response corresponds to a spring force, and the out-of-phase response corresponds to a damping force.

The force response can be characterized by the non-dimensional *squeeze number* $\sigma$. For a square plate of area $A = a^2$, driven sinusoidally by $e_o cos\omega t$, the squeeze number is given by

$$\sigma \;=\; \frac{12\mu a^2}{P_a h_m^2}\omega, \qquad (12)$$

where mean film thickness is $h_m$. For a 5 $\mu m$ thick air bearing, $10^{-6}m^2$ area platform, and drive frequency of $\omega = 10^5 s^{-1}$, the squeeze number is approximately $\sigma \approx 10$. For large squeeze numbers, the fluid layer has increased resistance to flowing out between the plates, increasing the effective stiffness of the air bearing.

The damping force $f_d$ is given by

$$f_d \;=\; \frac{128\sigma}{4\pi^6 \;+\; \sigma^2\pi^2}\frac{e_o}{h_m}P_a A \qquad (13)$$

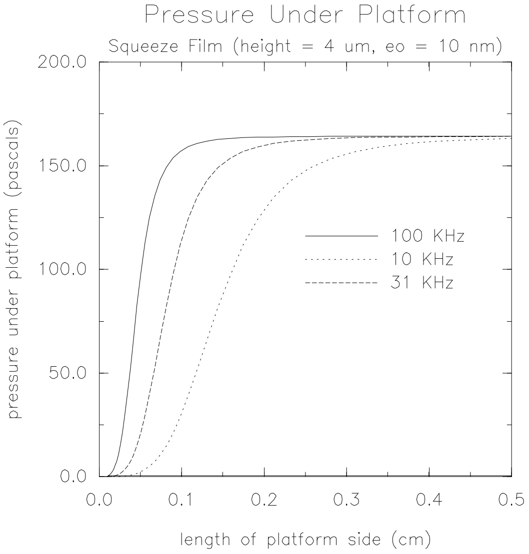


Figure 14: Theoretical pressure for various platform sizes, assuming 10 nm amplitude vibration. Note that a pressure of 100 pascal can support a piece of silicon about 4 mm thick. Parts less than 1 mm in size may drag on the substrate.

The spring force $f_k$ is given by

$$f_K \;=\; \frac{64\sigma^2}{4\pi^8 \;+\; \sigma^2\pi^4}\frac{e_o}{h_m}P_aA \tag{14}$$

The cutoff squeeze number $\sigma_c = 2\pi^2$ occurs when the spring and damping force are equal. At the cutoff squeeze number, the spring force is proportional to the inverse 5th power of the plate separation:

$$f_k \approx \frac{64\sigma^2}{8\pi^8}\frac{e_o}{h_m}P_aA = \frac{8}{\pi^8}\left(\frac{12\mu a^2}{P_a}\omega\right)^2\frac{e_o}{h_m^5}P_aA \tag{15}$$

while the damping force is proportional to the inverse cube of the float height. The squeeze-film bearing will resist the attraction of the platform to the substrate from gravitational and magnetic forces. Since $f_k$ is inversely proportional to the fifth power of the mean platform height, this bearing will be very stiff, but well damped due to the damping force $f_d$. With $\omega$ in the high audio range, a piezo-electric actuator can easily generate the required oscillation. See Figure 14 for trade-offs between platform size, pressure, and vibration frequency. See [Zhang et al 1992] for comparisons of theoretical and experimental results for squeeze film damping.

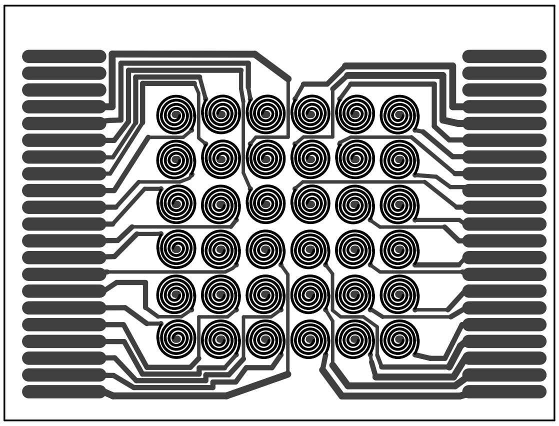

Figure 15: Electromagnet coil array. Coils are spaced 6.6 mm center-to-center. Copper traces are about $400\mu m$ wide and $30\mu m$ thick. Coil can handle 2 amps continuous duty without excessive temperature rise. Switching diodes and array connections are mounted on main control circuit board.

### 4.3 Squeeze Film Bearing Implementation

A piezo-electric transducer is used to drive the substrate in vertical oscillation, as shown in Figure 6. For stiff support of the weight of the platforms, the squeeze number $\sigma$ should be greater than the cutoff squeeze number $\sigma_c$. For small platforms, this implies that the drive frequency may need to be relatively high. The drive frequency should also be high enough to be inaudible. One limitation on the drive frequency is the excitation of bending modes in the substrate. These bending modes could easily have greater amplitude than the air bearing thickness. A relatively thick aluminum plate was chosen for its relatively high stiffness and low mass, with dimensions of approximately 5 by 3.5 cm. This size was chosen to provide complete support for the active sensor area of the substrate. The lowest bending mode [Timoshenko, Young, and Weaver, 1974] occurs at:

$$f_1 \;=\; \frac{\pi h_s}{a_s^2}\sqrt{\frac{E}{12\rho}} \quad , \tag{16}$$

where the density of aluminum is $\rho_{Al} = 2.7 \times 10^3 Kgm^{-3}$, the area $a_s^2$ is approximately $1.5 \times 10^{-3} m^2$, Young's Modulus is $E = 7 \times 10^{10} Nm^{-2}$,

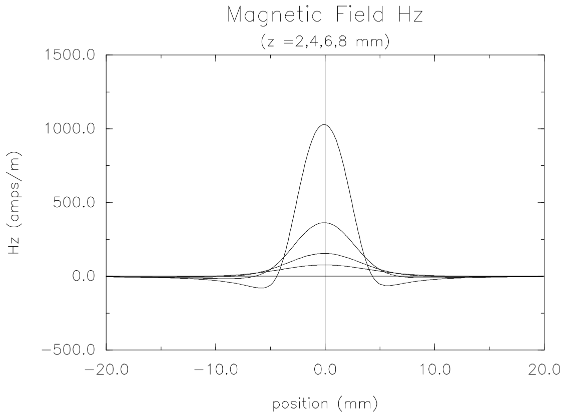


Figure 16: Relative vertical component of magnetic field for various heights above magnet. Because of the capacitive sensor array, the platform is approximately 2 mm above the electromagnets.

and the thickness of the substrate is $h_s \approx 1.2 \times 10^{-2} m$ which includes a glass covering layer over the capacitive array sensor. The first resonant frequency is then at about 40 KHz. We choose a drive frequency of 20KHz to reduce heat dissipation in the piezo drive, as the load of the platform, about 50 grams, is significant at such high frequencies.

# 5 Magnetic Actuator Design

The electro-magnet actuator consists of an array of planar coils fabricated on a printed circuit board as shown in Fig. 15. The coils are made of 2 layers of 4 turns of copper cladding, approximately 400 $\mu m$ in width and $30 \mu m$ thick. The coils are spaced 6.6 mm apart. (For comparison, Wagner and Benecke [1991] use a single coil of 17 turns in a 5.8 mm square.) A permanent magnet is attached to a 7.5 mm diameter glass or silicon platform, which is driven by the fields from the coil array. For a coil with current $I$ amps of negligible cross-section, the magnetic field is obtained from

$$\vec{H}(\vec{r}) = \frac{I}{4\pi} \int_l \frac{\vec{dl} \times \vec{r}}{|\vec{r}|^3} , \tag{17}$$

where $\mu_o$ is the permeability of free space, ($\mu_o = 4\pi \times 10^{-7} Hm^{-1}$), and $\vec{r}$ is the vector from the current element $I\vec{dl}$ to the calculation point. Using numerical integration, the $z$ component of the magnetic field is plotted in Figure 16, assuming 1.0 amp of current for heights of 2, 4, 6, and $8 \times 10^{-3}$m above the magnet surface. These heights are significant compared to the conductor size, thus ignoring the cross-section of conductors is reasonable. Note that the height of the platform above the magnetic layer includes the thickness of the capacitive array sensor.

For a permanent magnet with constant magnetization $\vec{M} = M_o \hat{z}$, the force per unit volume can be obtained (e.g. Jackson, [1975]) from

$$d\vec{F} = \nabla(\vec{M} \cdot \vec{B}) = M_o \nabla B_z = \mu_o M_o \nabla H_z , \tag{18}$$

where $B_z$ is the $z$ component of the magnetic flux density, and $H_z$ is the $z$ component of the magnetic field. Using a permanent magnet with a magnetic flux density of 1.0 Tesla, $M_o = 1.0T/\mu_o = 8 \times 10^5 ampm^{-1}$. Since the applied field strength is an order of magnitude less than the magnet's internal field, it is reasonable to assume a constant magnetization.

The total force is obtained from

$$\vec{F} = \int_{V_o} d\vec{F} dV . \tag{19}$$

The vertical force $F_z$ is supported by the air bearing, but may decrease the float height for large currents in the coil. Typically, the vertical forces are 10 times the horizontal force.

The torque per unit volume is obtained from

$$\vec{\tau} = \vec{M} \times \vec{B} = M_o \hat{z} \times \vec{B} = -M_o B_y \hat{x} + M_o B_x \hat{y} . \tag{20}$$

Note that with uniform vertical magnetization, there is no component of torque about the vertical axis. The torques about the horizontal axes may cause tilting of the platform, but the stiffness of the air bearing should prevent the platform from contacting the substrate.

The horizontal acceleration of the platform is limited by the gradient of the magnetic field and the magnetization of the permanent magnet. The horizontal force is given by

$$F_x = \int_{V_o} \mu_o M_o \frac{\partial H_z}{\partial x} \, dV . \tag{21}$$

A rough estimate of the force on the magnet can be made assuming an approximately constant field gradient at some position. With a current of 0.4 amp, the peak field gradient $\frac{\{\partial H_z\}}{\{\partial x\}}$ is approximately $1.2 \times 10^4 ampsm^{-2}$. Using $\mu_o M_o$ equal to

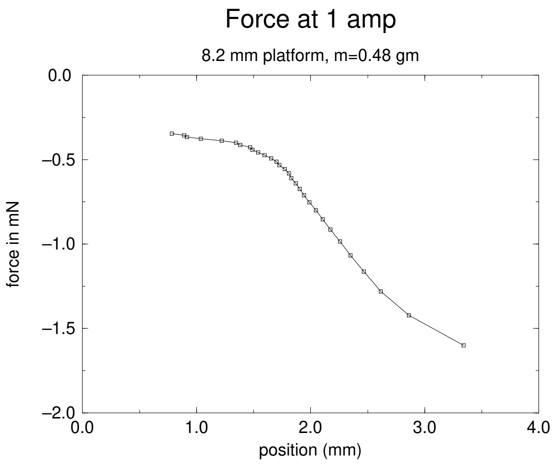


Figure 17: Force profile for platform on electromagnet with 1 amp.

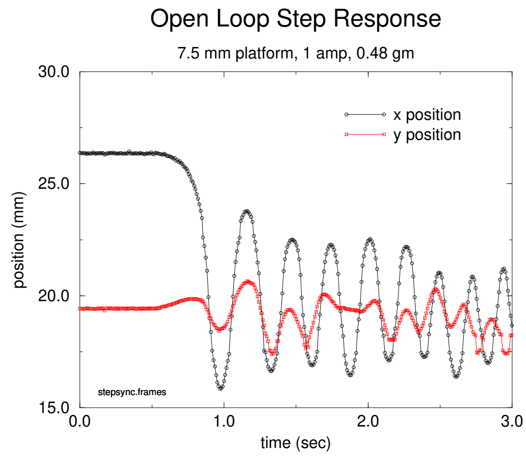


Figure 18: Open loop step response with 1 amp. Peak velocity $.15ms^{-1}$, and peak acceleration $\approx 3ms^{-2}$.

1.0 Tesla, the force per volume is $1.2 \times 10^4 Nm^{-3}$. A typical permanent magnet used is cylindrical, with diameter 6.3 mm and 5.0 mm length, for a total volume of approximately $1.6 \times 10^{-7} m^3$. The net force is then about $1.9 \times 10^{-3} N$. With a platform mass of $1.0 \times 10^{-3} Kg$, this gives an acceleration of about $2ms^{-2}$ which is quite reasonable for a workspace of less than $10cm^2$.

The static electromagnetic force on the platform can be measured as follows. We assume first that the magnetic field is circularly symmetric. The minimum force occurs when the platform is centered exactly above a magnet as can be seen by considering the gradient of Figure 16. The maximum force $f_{max}$ occurs at some distance say $r_{max} > 0$. When a constant force less than $f_{max}$ is applied to the platform, a stable equilibrium position will be reached which is a function of the current. Thus by applying a constant force and measuring the equilibrium position as a function of current, one can map out the force reponse of the system. A platform of mass 0.48 gram is placed on the air bearing at a tilt angle of 7.8 degrees. Thus the tangential force on the platform is a constant 0.64 mN. Figure 17 shows the measured force profile for this platform. The peak force occurs at a distance of about 3.3 mm from the coil center. This method can not be used to estimate the force profile at distances greater than $r_{max}$ since the system is unstable. With 1 amp, peak accelerations of $3ms^{-2}$ are predicted. (The coils can withstand 3 amps peak, and 2 amps continuous without overheating). Note that the force profile will be a function of the magnet dimensions.

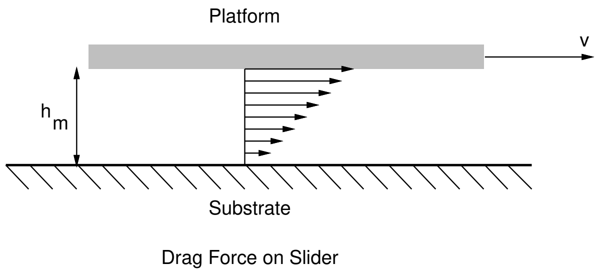


Figure 19: Drag force on slider.

The predicted accelerations are in line with what can be seen from measured step responses. A short portion of a 1 amp step response (open-loop) is shown in Figure 18. The natural frequency is on the order of 5 Hz, and damping ratio approximately 0.005. From Figure 17, the slope is approximately $0.5Nm^{-1}$ so the predicted natural frequency $\frac{1}{2\pi}\sqrt{\frac{k}{m}}$ of 5.1 Hz is in close agreement.

## 5.1 Drag Force Due to Air Bearing

Although the air bearing has no static friction component, it does contribute a velocity proportional damping term. Consider a platform moving at velocity $v = \dot{x}$ horizontally as in Figure 19. The relative velocity of the fluid at the fixed and moving surfaces should be zero, thus there is a shearing force on the platform due to the viscosity of air. This drag force is found from

$$F_{drag} \approx \frac{\mu A}{h_m}\dot{x} = b\dot{x} \qquad (22)$$

where viscosity for air is assumed to be $2 \times 10^{-5}\ Nsm^{-2}$, the platform area $A = 4.4 \times 10^{-5} m^2$. The damping ratio $\zeta = \frac{b}{2\sqrt{km}} \approx 0.006$ is in close agreement with the open loop step response. This result indicates that the air bearing is preventing any significant coulomb friction. Note that the power required to overcome this viscous drag is much less than $10^{-6} watt$. Another damping term to consider is the induced voltage in adjacent conductors due to the changing magnetic flux density.

# 6 Conclusions and Future Work

This paper has shown a relatively simple method to implement a miniature mobile platform system. With inherently low friction, position resolution is limited mainly by sensor noise. The almost pure-mass system is relatively easy to control. The coils can be scaled down somewhat using printed circuit technology, but lithographic techniques will probably be necessary to obtain a factor of 10 reduction in coil size.

The eventual goal of this work is to implement a micro-robot system consisting of a work surface and multiple planar micro-robots, which can autonomously move in the plane with three degrees-of-freedom. The micro-robots can work cooperatively to grasp and manipulate objects which may be larger than themselves. Eventually, a system with practical applications, such as assembly of micro-mechanical parts could be built. In the system concept, welding and inspection systems could be added at the periphery of the work surface, and parts could be shuttled between stations by the micro-robots, thus implementing a micro-assembly cell. Each micro-robot could be 1000 $\mu$m $\times$ 1000 $\mu$m in area, and only 100 $\mu$m thick. The micro-robot would rest on a fluid film (an air bearing) and never move while in frictional contact.

# Acknowledgments

I thank Steve Albrecht for layout and design of the printed circuit coil array and sensor array, and Emile Sahouria for implementing the multi-processor closed-loop control system. I also thank Hiroaki Furuichi and Michael Cohn for stimulating discussions.

# References

[1] C.H. Ahn, Y.J. Kim, and M.G. Allen, "A Planar Variable Reluctance Magnetic Micromotor with Fully Integrated Stator and Wrapped Coils" *Proc. IEEE Micro Electro Mechanical Systems*, pp. 1-6, Fort Lauderdale, FL Feb. 7-10, 1993.

[2] F. Arai, D. Ando, T. Fukuda, Y. Nonoda, and T. Oota, "Micro Manipulation Based on Micro Physics-strategy based on attractive force reduction and stress measurement", *Proc. IEEE/RSJ Intelligent Robots and Systems,* pp. 236-241, Pittsburgh, PA August 3-5, 1995.

[3] K. M. Anderson and J. Edward Colgate, "A model of the attachment/detachment cycle of electrostatic micro actuators", *ASME Micromechanical Sensors, Actuators, and Systems*, DSC-vol. 32, pp. 255-268, Atlanta, GA Dec. 1-6, 1991.

[4] M. Ataka, A. Omodaka, N. Takeshima, and H. Fujita, "Fabrication and Operation of a Polyimide Bimorph Actuators for a Ciliary Motion System", *Jnl. of Microelectromechanical Systems* , vol. 2, no. 4, pp. 146-150, Dec. 1993.

[5] J.J. Blech, "On Isothermal Squeeze Films", *ASME Jnl. of Lubrication Technology*, vol. 105, pp. 615-620, 1983.

[6] K. Boehringer, B.R. Donald, R. Milhailovich, N.C. MacDonald, "Sensorless Manipulation Using Massively Parallel Microfabricated Actuator Arrays", *IEEE Int. Conf. on Robotics and Automation* , pp. 826-833, San Diego: May 8-13, 1994.

[7] M.H.W. Bonse, F. Zhu, and J.W. Spronck, "A New Two Dimensional Capacitive Position Transducer", *Sensors and Actuators* , vol. 41-42, pp. 29-32, 1994.

[8] I.J. Busch-Vishniac, S. Chen, M. Jeong, S. Li, and I. Wang, "Magnetic Levitation-Based Micro-Automation of Mechanical Processes in Semiconductor Fabrication", *Proc. IEEE Micro Electro Mechanical Systems*, pp. 142-146, Napa Valley, CA, Feb. 1990.

[9] I.J. Busch-Vishniac, "The Case for Magnetically Driven Micro-Actuators", *ASME Micromechanical Sensors, Actuators, and Systems,*DSC-vol. 32, pp. 287-302, Atlanta, GA Dec. 1-6, 1991.

[10] P. Dario, R. Valleggi, M.C. Carrozza, M.C. Montesi, and M. Cocco, "Microactuators for microrobots: a critical survey", *J. Micromech. Microeng.* vol. 2, pp. 141-157, 1992.

[11] R.S. Fearing, "A Miniature Mobile Platform on an Air Bearing", *Third Int. Symp. on Micro Machine and Human Sciences*, Oct. 14-16, 1992, Nagoya, Japan.

[12] G. Fuhr, R. Hagedorn, T. Muller, B. Wegner, and W. Benecke, "Linear Motion of Dielectric Particles and Living Cells in Microfabricated structures induced by traveling electric fields", *IEEE Micro Electro Mechanical Systems"*,Nara, Japan, Feb. 1991, pp. 259-264.

[13] H. Fujita, "Studies of Micro-Actuators in Japan", *IEEE Int. Conf. on Robotics and Automation*, Scottsdale, AZ, May 1989, pp. 1559-1564.

[14] H. Fujita and A. Omodaka, "Electrostatic Actuators for Micromechatronics", *IEEE MicroRobots and Teleoperators Workshop,* Hyannis, MA Nov. 9-11, 1987.

[15] H. Fujita and Kaigham J. Gabriel, "New Opportunities for MicroActuators", 1991 Int. Conf. on Solid-State Sensors and Actuators (Transducers '91) June 1991, San Francisco, CA, pp. 14-20.

[16] T. Fukuda and T. Tanaka, "Micro-Electro Static Actuator with Three Degrees of Freedom", *Proc. of the IEEE Workshop on Micro-Electro Mechanical Systems* , Napa Valley, CA Feb. 11-14, 1990.

[17] T. Furuhata, T. Hirano, and H. Fujita, "Array-Driven Ultrasonic Microactuators- arrayed microactuator modules that have swing pins", 1991 Int. Conf. on Solid-State Sensors and Actuators (Transducers '91), June 1991, San Francisco, CA, pp. 1056-1059.

[18] H. Guckel, T.R. Christenson, K.J. Skrobis, T.S. Jung, J. Klein, K.V. Hartojo, and I. Widjaja, "A First Functional Current Excited Planar Rotational Magnetic Micromotor", *Proc. IEEE Micro Electro Mechanical Systems*, pp. 7-11, Fort Lauderdale, FL Feb. 7-10, 1993.

[19] W.R. Harper, *Contact and frictional electrification*, Oxford: Clarendon Press, 1967.

[20] R.G. Horn, D.T. Smith, "Contact electrification and adhesion between dissimilar materials." *Science*, 17 April 1992, vol.256, (no.5055):362-4.

[21] T. Inoue, K. Iwatani, I. Shimoyama and H. Miura, "Micromanipulation Using Magnetic Field", *IEEE Int. Conf. Robotics and Automation* , pp. 679-684, Nagoya, Japan May 1995.

[22] J. Ish-Shalom, "Sawyer Sensor for Planar Motion Systems", *IEEE Int. Conf. on Robotics and Automation* , pp. 2652-2658, San Diego, CA, May 8-13, 1994

[23] J.D. Jackson, *Classical Electrodynamics*, 2nd ed., Wiley:New York, 1975.

[24] Y. Kim, M. Katsurai, and H. Fujita, "Fabrication and Testing of a Micro Superconducting Actuator using the Meissner Effect", *Proc. IEEE Micro Electro Mechanical Systems*, pp. 61-66, Napa Valley, CA, Feb. 1990.

[25] S. Konishi and H. Fujita, "A Conveyance System Using air flow based on the concept of distributed micro motion systems", *7th Int. Conf on Solid-State Sensors and Actuators (Transducers '93)* , pp. 28-31, Yokohama, Japan, June 1993.

[26] C. Liu, T. Tsao, and Y.-C. Tai, "Out of Plane Permalloy Magnetic Actuators for Delta-Wing Control", *Proc. IEEE Micro Electro Mechanical Systems* , pp. 7-12, Amsterdam Jan. 29-Feb 2, 1995.

[27] W. Liu and P. Will, "Parts Manipulation on an Intelligent Motion Surface", *Proc. IEEE-RSJ Intelligent Robots and Systems*, pp. 399-404, Pittsburgh, PA August 3-5, 1995.

[28] Y. Maeda, K. Aihara, and H. Fujita, "A Vacuum-compatible X-Y micro-actuator using the levitational effect of a superconductor" *Robotics, Mechatronics and Manufacturing Systems*, ed. by T. Takamori and K. Tsuchiya, North-Holland Elsevier 1993, pp. 509-514.

[29] G.L. Miller, "Capacitive Incremental Position Measurement and Motion Control", United States Patent 4893071, Jan. 9, 1990.

[30] F.M. Moesner and T. Higuchi, "Devices for Particle Handling by an AC Electric Field" *Proc. IEEE Micro Electro Mechanical Systems* , pp. 66-71, Amsterdam Jan. 29-Feb 2, 1995.

[31] C.H.T. Pan and P.H. Broussard, "Squeeze-Film Lubrication", Proc. Gas Bearing Symposium on Design Methods and Applications, pp. 12/1-12/35, Univ. of Southampton, April 1967.

[32] K.S.J. Pister, M.W. Judy, S.R. Burgett, and R.S. Fearing, "Microfabricated Hinges", *Sensors and Actuators A*,vol. 33, pp. 249-256, 1992.

[33] K.S.J. Pister, R.S. Fearing, and R.T. Howe, "A Planar Air Levitated Electrostatic Actuator System", *IEEE Workshop on Micro Electro Mechanical Systems*, Napa Valley, CA Feb. 12-14 1990.

[34] R.H. Price, J.E. Wood, and S.C. Jacobsen, "Modelling Considerations for Electrostatic Forces in Electrostatic Microactuators", *Sensors and Actuators* , vol. 20, pp. 107-114, 1989.

[35] J. Robichaux and S. Ahmed, "Magnetically Levitated Micro-Robots: Design, Control, Experimentation and Applications", *Robotics and Manufacturing: recent trends in research, education, and applications, Proc. of the 4th Int. Symp. on Robotics and Manufacturing* , Nov. 11-13, 1992, Sante Fe NM pp. 9-14.

[36] K. Sato, Y. Kawamura, S. Tanaka, K. Uchida, and H. Kohida, "Individual and Mass Operation of Biological Cells using Micromechanical Silicon Devices", *Sensors and Actuators*, vol. A21-A23, pp. 948-953, 1990.

[37] F.S. Sherman, *Viscous Flow*, McGraw-Hill, New York: 1990.

[38] I. Shimoyama, "Scaling in Microrobots", *Proc. IEEE/RSJ Intelligent Robots and Systems* , pp. 208-211, Pittsburgh, PA August 3-5, 1995.

[39] K. Suzuki, H. Miura, I. Shimoyama and Y. Ezura, "Creation of an Insect-based Microrobot with an External Skeleton and Elastic Joints", *Proc. IEEE Micro Electro Mechanical Systems Workshop,* Travemunde, Germany, February 4-7, 1992, pp. 190-195.

[40] H. Tokisue, N. Tsumaki, H. Inoue, and M. Tsukagoshi, "Development of Wafer Handling Systems in Gas, Liquid and Vacuum Environments for ULSI Manufacturing", *Proc. 69th JSME Fall Annual Meeting*, pp. 354-356, Nagoya, Japan, Oct. 16-17, 1991.

[41] W. Trimmer and R. Jebens, "Actuators for Micro Robots", IEEE Intern. Conf. on Robotics and Automation, Scottsdale, AZ, May 1989, pp. 1547-1552.

[42] B. Wagner, M. Kreutzer, and W. Benecke, "Permanent Magnet Micromotors on Silicon Substrates", *Jnl. of Microelectromechanical Systems* , vol. 2, no. 1, pp. 23-29, 1993.

[43] B. Wagner and W. Benecke, "Microfabricated Actuator with Moving Permanent Magnet", *Proc. IEEE Micro Electro Mechanical Systems* , pp. 27-32, Nara, Japan, Feb. 1991.

[44] B. Wagner, M. Kreutzer, and W. Benecke, "Electromagnetic MicroActuators with Multiple Degrees of Freedom" 1991 Int. Conf. on Solid-State Sensors and Actuators (Transducers '91), June 1991, San Francisco, CA, pp. 614-617.

[45] I. A. Wang, S. Li, and I. Busch-Vishniac, "A Magnetic Levitation Transport Path" *IEEE Trans. on Semiconductor Manufacturing*, vol. 4, no.2, May 1991.

[46] M. Washizu, "Electrostatic Manipulation of Biological Objects in Microfabricated Structures", *Integrated Micro-Motion Systems: Micromachining, Control, and Applications*, Proc. Third Toyota Conference, Aichi, Japan, 22-25 Oct. 1989, pp. 417-431.

[47] L. Zhang, D. Cho, H.Shirashi, and W. Trimmer, "Squeeze film damping in microelectromechanicl systems", in *Micromechanical Systems* , Winter Annual Meeting ASME DSC-Vol. 40, Anaheim, CA Nov. 8-13, 1992 pp. 149-160.